REPORT DOCUMENTATION PAGE

Public reporting burden for this collection of information is estimated to average 1 hour per response, including the time for reviewing data needed, and completing and reviewing this collection of information. Send comments regarding this burden estimate or any other his burden to Department of Defense, Washington Headquarters Services, Directorate for Information Operations and Reports (0704 1302. Respondents should be aware that notwithstanding any other provision of law, no person shall be subject to any penalty for fai valid OMB control number. PLEASE DO NOT RETURN YOUR FORM TO THE ABOVE ADDRESS.

AFRL-SR-BL-TR-01-

0187

1. REPORT DATE (DD-MM-YYYY)	2. REPORT TYPE	3. DATES COVERED (From - To)
15-01-2001	Final Report	01-07-1997 - 30-06-2000

4. TITLE AND SUBTITLE

Fellowships for the advancement of large-eddy simulations

5a. CONTRACT NUMBER
F49620-97-1-0478

5b. GRANT NUMBER

5c. PROGRAM ELEMENT NUMBER

5. AUTHOR(S)

Kenneth Jansen and Andres Tejada-Martinez

5d. PROJECT NUMBER

5e. TASK NUMBER

5f. WORK UNIT NUMBER

7. PERFORMING ORGANIZATION NAME(S) AND ADDRESS(ES)

Rensselaer Polytechnic Institute
110 8th Street
Troy, NY 12180-3590

8. PERFORMING ORGANIZATION REPORT NUMBER

A10804

9. SPONSORING / MONITORING AGENCY NAME(S) AND ADDRESS(ES)

AFOSR/NA
810 N. Randolph Street, Room 732
Arlington, VA 22203-1977

10. SPONSOR/MONITOR'S ACRONYM(S)

11. SPONSOR/MONITOR'S REPORT NUMBER(S)

12. DISTRIBUTION / AVAILABILITY STATEMENT

Approved for public release; distribution is unlimited.

AIR FORCE OFFICE OF SCIENTIFIC RESEARCH (AFOSR)
NOTICE OF TRANSMITTAL DTIC. THIS TECHNICAL REPORT
HAS BEEN REVIEWED AND IS APPROVED FOR PUBLIC RELEASE
LAW AFR 190-12. DISTRIBUTION IS UNLIMITED.

13. SUPPLEMENTARY NOTES

14. ABSTRACT

In many complex flows, large-eddy simulation is difficult due to the simultaneous presence of a variety of flow features, often with quite different resolution requirements. For this reason, unstructured-grid large-eddy simulation techniques are being developed using the finite element method to solve the compressible Navier-Stokes equations with a dynamic model of the subgrid-scale stresses. As the purpose of this report was to support graduate student education, the bulk of this report is taken from the work of the student supported by this research (Andres Tejada-Martinez). That student has focused on the characterization of filters used within the dynamic subgrid-scale model for large eddy simulation. Though he is not quite finished, this report clearly shows that much was learned under the three years of support by the AFOSR.

15. SUBJECT TERMS

16. SECURITY CLASSIFICATION OF:			17. LIMITATION OF ABSTRACT	18. NUMBER OF PAGES	19a. NAME OF RESPONSIBLE PERSON
a. REPORT	b. ABSTRACT	c. THIS PAGE			Kenneth E. Jansen
U	U	U	UU	23	19b. TELEPHONE NUMBER (include area code) (518) 276-6755

Final report for AASERT grant entitled

Fellowships for the advancement of large-eddy simulation

Agreement # F49620-97-1-0478

Submitted by:

Kenneth Jansen and Andres Tejada Martinez
Department of Mechanical Engineering,
Aeronautical Engineering and Mechanics
Rensselaer Polytechnic Institute

Submitted to:

Air Force Office of Scientific Research

For the period

July 1, 1997 - June 30, 2000

20010402 120

Abstract

In many complex flows, large-eddy simulation is difficult due to the simultaneous presence of a variety of flow features, often with quite different resolution requirements. For example, a typical flow over an airfoil near maximum lift includes laminar, transitional, and turbulent boundary layers, flow separation, unstable free shear layers and a wake. In such situations, unstructured-grid methods can gain great efficiencies over structured-grid methods (factor of 27) by placing points based on local resolution requirements, rather than along lines (as is required with structured-grid methods). For this reason, unstructured-grid large-eddy simulation techniques are being developed using the finite element method to solve the compressible Navier-Stokes equations with a dynamic model of the subgrid-scale stresses. As the purpose of this report was to support graduate student education, the bulk of this report is taken from the work of the student supported by this research (Andres Tejada-Martinez) . That student has focused on the characterization of filters used within the dynamic subgrid-scale model for large eddy simulation. Though he is not quite finished, this report clearly shows that much was learned under the three years of support by the AFOSR. This grant also allowed partial support for Michael Yaworski. He is currently finishing his masters in RANS simulations and will go on to link Andres work to combined LES/RANS models. We have decided to present only Andres work here in the interest of completeness and compactness.

1 Introduction

Large-eddy simulation (LES) is a technique for computation of turbulent flows where the large-scale component of the flow, carrying most of the energy, is resolved by the computational method, and the small-scale field motions are modeled. Previous to LES, the two major approaches to simulating turbulent flows were Direct Numerical Simulation (DNS) and Reynolds-Averaged Navier-Stokes Simulation (RANSS). In DNS, the computational method resolves all of the turbulent motions from the largest scale down to the scale where motion is converted to heat via viscous dissipation. It is well known that DNS is limited to low Reynolds number flows due to the increasing range of small scales with increasing Reynolds number. In RANSS, the space-time computational grid is too coarse to resolve the flow instabilities that lead to and characterize turbulence. The grid is only fine enough to resolve the mean flow, thereby requiring some type of modeling of the statistical effects of all turbulent fluctuations on the mean flow. LES is a compromise between DNS and RANSS. The computational grid is sufficiently fine to resolve some flow instabilities, but not fine enough to resolve the energy-dissipating motions. The idea behind LES is that motions that are resolved are the important ones and the errors induced by modeling the small-scale motions are significantly smaller than those incurred in RANSS. The constant coefficient Smagorinsky model (see [15]), analogous to the linear viscosity model in RANSS, is often used to account for the un-resolved small-scale motions. A more accurate procedure is often used in which the constant coefficient model becomes a dynamic coefficient model as the model coefficient is no longer taken as constant but allowed to vary in space and time.

Over the past three decades, a significant amount of research has been devoted to LES beginning with Lilly [7] who adopted LES to predict flows in the field of Meteorology. The overwhelming majority of this research has been carried out with spectral or structured grid finite difference methods. However, recently LES has been extended to finite element methods on unstructured grids (see [4]). This extension not only facilitates simulation of flows within or around complex geometries, but also allows great reductions in computational effort through the ability of unstructured grids to adapt locally to resolve fine-scale flow structures in one flow region while remaining coarse in other regions where the flow structures are large.

The purpose of this report is to investigate the extension of LES to finite elements by focusing on the intricacies arising from such a task. In Section 2, we present classical definitions of spatial filters along with their relevant characteristics for LES. In Sections 3 and 4, we review the filtered Navier-Stokes equations (which govern the large-scale component of the flow) along with the dynamic coefficient Smagorinsky model required to represent unknowns in the filtered equations generated by a filtering operation. In Section 5, we discuss discrete filters which arise when the modeled filtered Navier-Stokes equations are solved using finite elements, and furthermore we introduce new filters which make use of the basis functions underlying the numerical method, referred to as finite dimensional filters. Finally, in Section 6 we test our discrete and finite dimensional filters by performing large-eddy simulations of decaying isotropic

turbulence and comparing the results with experimental data.

2 Filtering

In the large-eddy simulation (LES) of turbulent flows, the larger unsteady turbulent motions (or eddies) are directly represented, whereas the effects of the smaller-scale motions are modeled. There are four conceptual steps in LES:

1. A filtering operation is defined to decompose the velocity $\boldsymbol{u}(\boldsymbol{x},t)$ into the sum of a filtered (or resolved) component $\bar{\boldsymbol{u}}(\boldsymbol{x},t)$ and a residual or subgrid scale (SGS) component $\boldsymbol{u}'(\boldsymbol{x},t)$. The filtered component represents the motions of the large eddies.
2. The evolution equations for the filtered velocity field are derived from the Navier-Stokes equations. These equations are of the same form as the Navier-Stokes equations, with the momentum equation containing an unknown residual (SGS) stress tensor that arises from the residual motions.
3. Closure is obtained by modeling the residual stress tensor; in our case, the dynamic coefficient Smagorinsky model is used.
4. The modeled filtered equations are solved numerically for $\bar{\boldsymbol{u}}(\boldsymbol{x},t)$, which provides an approximation to the large-scale motions of the turbulent flow.

The general filtering operation, introduced to LES by Leonard [6], is defined as

$$\bar{\boldsymbol{u}}(\boldsymbol{x},t) = \int G(\boldsymbol{x},\boldsymbol{y})\, \boldsymbol{u}(\boldsymbol{y},t)\, d\boldsymbol{y}, \tag{1}$$

where integration is over the entire flow domain. The filter kernel $G(\boldsymbol{x},\boldsymbol{y})$, located at $\boldsymbol{y}=\boldsymbol{x}$, is chosen to have small compact support in $\boldsymbol{y}$ thereby reducing the region of integration to be much smaller than the flow domain. The simplest filter kernels are spatially homogeneous, symmetric in $\boldsymbol{y}$ about $\boldsymbol{x}$ (leading to the expression of G as $G(|\boldsymbol{x}-\boldsymbol{y}|)$), and are required to satisfy the following normalization condition:

$$\int G(\boldsymbol{r})\, d\boldsymbol{r} = 1, \tag{2}$$

guaranteeing that the filtering operation preserves constants. Homogeneity simply refers to the fact that the shape of the kernel remains constant as we move the point $\boldsymbol{y}=\boldsymbol{x}$.

Symmetric filter kernels can be defined in one dimension. The extension to the three dimension vector case is straight forward. Two commonly used homogeneous, non-negative, symmetric filters are the box filter and the Gaussian filter. Consider a random function $f(x)$ characterized by high frequencies. With the box filter, the filtered function $\bar{f}(x)$ is simply the average of $f(x)$ in the interval $(x-\Delta/2, x+\Delta/2)$. Thus the box filter kernel takes on the value of $1/\Delta$ over the previously mentioned interval and is zero elsewhere. The Gaussian filter kernel is the Gaussian distribution with mean zero and variance $\sigma^2 = \Delta^2/12$. This value of the variance was chosen by Leonard so as to match the second moment of the Gaussian filter kernel to that of the box filter kernel.

A box or Gaussian filtered function $f(x)$ follows the general trends of $f(x)$, but the short fluctuations of length scales smaller than Δ have been damped. This admits a natural way of categorizing filters by their widths, taken as Δ. Just like the Gaussian filter, other non-negative, symmetric filters are required to match their second moments with that of the box filter, resulting in the following general definition of their widths:

$$\Delta = \left(12 \int_{-\infty}^{\infty} r^2 G(r)\, dr\right)^{1/2}. \tag{3}$$

This definition is extensively discussed by Lund [9]. The previous formula will be of interest to us when defining discrete filtering procedures for the dynamic Smagorinsky model.

3 The filtered Navier-Stokes equations

The incompressible Navier-Stokes equations are

$$\begin{aligned} \frac{\partial u_i}{\partial x_i} &= 0 \\ \frac{\partial u_i}{\partial t} + \frac{\partial u_j u_i}{\partial x_j} &= \nu \frac{\partial^2 u_i}{\partial x_j \partial x_j} - \frac{1}{\rho}\frac{\partial p}{\partial x_i}, \end{aligned} \tag{4}$$

where the first equation describes conservation of mass and the second equation describes conservation of momentum in the i-th direction. As usual, $u_i(\boldsymbol{x}, t)$ is the component of the velocity field in the i-th direction, $p(\boldsymbol{x}, t)$ is the pressure, ρ is the fluid density and ν is the kinematic viscosity. Consider the application of any homogeneous, symmetric filter with kernel $\bar{G}$ and of width $\bar{\Delta}$. Consequently, the filtered Navier-Stokes equations are rendered as:

$$\begin{aligned} \frac{\partial \bar{u}_i}{\partial x_i} &= 0 \\ \frac{\partial \bar{u}_i}{\partial t} + \frac{\partial \overline{u_j u}_i}{\partial x_j} &= \nu \frac{\partial^2 \bar{u}_i}{\partial x_j \partial x_j} - \frac{1}{\rho}\frac{\partial \bar{p}}{\partial x_i}. \end{aligned} \tag{5}$$

As can be seen, the filtering operation commutes with differentiation, which is brought about by the homogeneity of the kernels in question. The equations in (5) differ from the Navier-Stokes equations because the filtered product $\overline{u_i u_j}$ is different from the product of the filtered velocities $\bar{u}_i \bar{u}_j$. The difference is the residual or subgrid scale stress tensor defined by

$$\tau_{ij} = \overline{u_i u}_j - \bar{u}_i \bar{u}_j. \tag{6}$$

Expressing the deviatoric or traceless part of this tensor as

$$\tau_{ij}^d = \tau_{ij} - \frac{1}{3}\tau_{kk}\delta_{ij}, \tag{7}$$

and adding the trace of the residual stress tensor multiplied by the density to the pressure as

$$\bar{P} = \bar{p} + \rho\, \frac{1}{3}\tau_{kk}, \tag{8}$$

the filtered momentum equation in (5) can be rewritten as

$$\frac{\partial \bar{u}_i}{\partial t} + \frac{\partial \bar{u}_j \bar{u}_i}{\partial x_j} = \nu \frac{\partial^2 \bar{u}_i}{\partial x_j \partial x_j} - \frac{\partial \tau_{ij}^d}{\partial x_j} - \frac{1}{\rho} \frac{\partial \bar{P}}{\partial x_i}. \tag{9}$$

If $\tau_{ij}^d(\boldsymbol{x}, t)$ is given by a residual stress model, the filtered continuity equation (the first equation in (5)) and the filtered momentum equation (9), herein referred to as the filtered Navier-Stokes equations, can be solved to determine $\bar{\boldsymbol{u}}(\boldsymbol{x}, t)$ and $\bar{P}(\boldsymbol{x}, t)$.

In the case of compressible flows, the compressible Navier-Stokes equations are filtered using a generalized filtering procedure known as Favre (or density weighted) filtering. The interested reader is encouraged to consult Moin *et al* [10].

4 The dynamic Smagorinsky model

The filter applied to the Navier-Stokes equations is meant to remove the small scales of motion. Motion is converted to heat via viscous dissipation at the smallest of these small scales. Thus, the dissipation of motion must be modeled due to the absence of the smallest scales. Fortunately, by Kolmogorov's first hypothesis (see [12]), the behavior of the absent smallest (or Kolmogorov) scales is universal, and as a result, it should be possible to construct a model applicable to all types of flows. A simple model was proposed by Smagorinsky [15] to account for the dissipation of motion. Smagorinsky expressed the deviatoric portion of the residual stress tensor as

$$\tau_{ij}^d = -2(C\bar{\Delta})^2 |\bar{S}| \bar{S}_{ij}, \tag{10}$$

where C is the Smagorinsky coefficient, the filtered strain rate tensor is defined as

$$\bar{S}_{ij} = \frac{1}{2} \left(\frac{\partial \bar{u}_i}{\partial x_j} + \frac{\partial \bar{u}_j}{\partial x_i} \right), \tag{11}$$

and the norm of the filtered strain rate tensor is defined as

$$|\bar{S}| = (2\bar{S}_{ij}\bar{S}_{ij})^{1/2}. \tag{12}$$

Note that (10) is consistent in the sense that its left hand side and its right hand are traceless. The previous model is valid only if the filter width, $\bar{\Delta}$, is in the inertial sub-range. Scales in the inertial sub-range are larger than the Kolmogorov scales, yet smaller than the scales which contain most of the energy. Moreover, the inertial sub-range scales are universal and, unlike the Kolmogorov scales, are not affected by molecular viscosity. The reason for the restriction on $\bar{\Delta}$ is that, by construction, the Smagorinsky model represents all the dissipation of motion occurring at the Kolmogorov scales. If some of these scales are preserved by the filter, then the dissipation of motion occurring at these scales will be accounted by the model as well. This is clearly incorrect. A final characteristic of the Smagorinsky model is that it is not suitable to represent the possible energy transfers from the removed Kolmogorov scales

to the larger scales, a phenomenon known as *backscatter*. The reason for such deficiency is that *backscatter* occurs on time scales smaller than those represented by the model. Currently, we are implementing a model which can exhibit *backscatter*, known as the Bardina mixed-scale model (see [16] and [19])).

One of the problems with the implementation of the Smagorinsky model is that the appropriate value of the coefficient C is different in different flow regimes. More precisely, it is zero in laminar flow, and it is attenuated near walls compared to its value ($C \approx 0.15$) in high Reynolds number free turbulent flows. To alleviate this deficiency of the constant coefficient model, Germano [3] developed a procedure for calculating the coefficient locally. Consider the application of a homogeneous, symmetric, secondary or test filter (with kernel $\hat{G}$ and of width $\hat{\Delta} > \bar{\Delta}$ in the inertial sub-range) to the once filtered Navier-Stokes equations. As expected, the continuity and momentum equations take the form:

$$\begin{aligned} \frac{\partial \hat{\bar{u}}_i}{\partial x_i} &= 0 \\ \frac{\partial \hat{\bar{u}}_i}{\partial t} + \frac{\partial \widehat{\bar{u}_j \bar{u}_i}}{\partial x_j} &= \nu \frac{\partial^2 \hat{\bar{u}}_i}{\partial x_j \partial x_j} - \frac{1}{\rho} \frac{\partial \hat{\bar{p}}}{\partial x_i}. \end{aligned} \tag{13}$$

The residual stresses created by the application of the test filter are expressed as

$$T_{ij} = \widehat{\bar{u}_i \bar{u}_j} - \hat{\bar{u}}_i \hat{\bar{u}}_j. \tag{14}$$

The successive application of two homogeneous filters of widths $\bar{\Delta}$ and $\hat{\Delta}$ respectively, yields a homogeneous filter with kernel $\hat{\bar{G}}$ and of width $\hat{\bar{\Delta}} > \bar{\Delta}$ (see [12] and [17]). (see [16] and [18]). Thus the Smagorinsky model for the deviatoric portion of the residual stresses in (14) takes shape as

$$T_{ij}^d = T_{ij} - \frac{1}{3} T_{kk} \delta_{ij} = -2(C\hat{\bar{\Delta}})^2 |\hat{\bar{S}}| \hat{\bar{S}}_{ij}, \tag{15}$$

where $\hat{\bar{S}}_{ij}$ and $|\hat{\bar{S}}|$ are defined straightforwardly based on $\hat{\bar{u}}$. Moreover, C is the same constant appearing in (10), a consequence of Kolmogorov's hypothesis mentioned earlier.

An identity due to Germano is obtained by applying the test filter to (6) and subtracting the result from (14):

$$L_{ij} = T_{ij} - \hat{\tau}_{ij} = \widehat{\bar{u}_i \bar{u}_j} - \hat{\bar{u}}_i \hat{\bar{u}}_j. \tag{16}$$

The significance of this identity is that L_{ij} (called the resolved stress tensor) is known in terms of $\bar{u}$, whereas T_{ij} and τ_{ij} are not. Taking the Smagorinsky coefficient as roughly constant in the neighborhood where the filter kernel is non-zero, the relations in (10) and (15) lead to

$$L_{ij}^d = T_{ij}^d - \hat{\tau}_{ij}^d = 2(C\bar{\Delta})^2 M_{ij}, \tag{17}$$

where L_{ij}^d is the deviatoric portion of L_{ij}:

$$L_{ij}^d = L_{ij} - \frac{1}{3} L_{kk} \delta_{ij}, \tag{18}$$

and

$$M_{ij} = \widehat{|\bar{S}|\bar{S}_{ij}} - \left(\frac{\hat{\bar{\Delta}}}{\bar{\Delta}}\right)^2 |\hat{\bar{S}}|\hat{\bar{S}}_{ij}. \tag{19}$$

The coefficient $(C\bar{\Delta})^2$ cannot be chosen to match the six independent relations in (17), but as shown by Lilly [8], the mean-square error is minimized by the specification that

$$(C\bar{\Delta})^2 = \frac{1}{2}\frac{M_{ij}L_{ij}^d}{M_{kl}M_{kl}} = \frac{1}{2}\frac{M_{ij}L_{ij}}{M_{kl}M_{kl}}. \tag{20}$$

The second equality in the previous expression arises from the fact that M_{ij} is traceless. Finally, both L_{ij} and M_{ij} are known in terms of $\bar{\boldsymbol{u}}(\boldsymbol{x}, t)$, thereby completing the expression in (10).

The denominator and numerator in (20) are averaged over homogeneous directions of the flow (i.e.,. directions over which mean quantities of the flow are constant) resulting in a time dependent Smagorinsky coefficient as a function of the directions in which the flow is not homogeneous. Averaging is an *ad hoc* operation performed as a way to avoid instabilities. In some instances, the fluctuations of M_{ij} between negative and positive values result in a vanishing of the denominator in (20). Furthermore, a negative value of $(C\bar{\Delta})^2$ would give rise to a parasitic transfer of energy from the modeled smallest scales to the larger scales. We refer to this transfer of energy as parasitic because, as mentioned earlier, the Smagorinsky model is not able to describe such transfers (*backscatter*).

5 Test filtering

Before we begin our discussion on test filtering, it is necessary to mention the numerical method used to solve the filtered Navier-Stokes equations. The spatial discretization in our large-eddy simulations is brought about by the Galerkin approximation to the weak form of the filtered Navier-Stokes equations augmented by the Streamline Upwind Petrov-Galerkin (SUPG) stabilization, herein referred to as the stabilized Galerkin approximation (see [4] and [18]). The spatially discretized equations are advanced in time using the generalized-α time integrator discussed in reference [5]. The stabilized Galerkin approximation involves the representation of the flow variables as a linear combination of continuous piecewise polynomial basis functions of order p. In turn, these velocity fields are used to calculate the dynamic model, which requires the test filtering of numerous flow quantities including the product of two components of the velocity (see (16)). For example, if $p = 1$ these flow quantities are products of the piecewise tri-linear linear velocity fields, thus they will be piecewise tri-quadratics or higher.

5.1 The box filter as the test filter

Performing the filtering integrations using the box filter kernel (of width $\bar{\Delta} = 2h$ where h is the constant mesh spacing) integrated by different quadrature rules

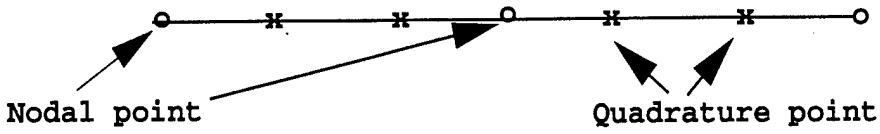

Figure 1: A nodal point with neighboring quadrature points are depicted. Test filtered quantities are calculated at the nodes.

admits a family of discrete approximations to a box filtered function evaluated at a particular node in the mesh. In one-dimension, this family can be represented as

$$\hat{f}(x_0) = \sum_{i=-J}^{J} W_i f(x_i). \tag{21}$$

Here the filtered function $\hat{f}(x)$ is evaluated at a mesh node whose spatial location is denoted as x_0 with neighboring quadrature points located at $x_1 = x_0 + L_1$, $x_2 = x_0 + L_2, \cdots, x_J = x_0 + L_J$ to the right and $x_{-1} = x_0 - L_1$, $x_{-2} = x_0 - L_2, \cdots, x_{-J} = x_0 - L_J$ to the left, where the $\{L_i\}$ are constants determined by the quadrature rule and the mesh spacing h.

The $\{L_i\}$ are representable in the form $L_i = \alpha_i h$ where $0 < \alpha_i < 1$. Furthermore, the weights are non-negative, symmetric (i.e., $W_i = W_{-i}$), and satisfy the condition

$$\sum_{i=-J}^{J} W_i = 1. \tag{22}$$

Therefore, this family of discrete filters preserves constants. An example of a discrete approximation to the box filter is given in Appendix I. The family of discrete kernels corresponding to the family of discrete filters applied in (21) can be expressed as

$$\hat{G}(x - y) = h \sum_{i=-J}^{J} W_i \delta(x - y + \alpha_i), \tag{23}$$

where $\alpha_{-i} = -\alpha_i$ and $\delta(x)$ is the Dirac delta function. The previous relation can be inserted into (3) to obtain a general expression for the filter width:

$$\hat{\Delta} = h \left(12 \sum_{i=-J}^{J} W_i \alpha_i^2 \right)^{1/2}. \tag{24}$$

It is important to note that the width of the discrete filters is proportional to the mesh size h. Thus, if the mesh is too coarse, the width of these discrete filters might be too wide for consistent calculation of the dynamic model. Recall that the width of the test filter should be within the inertial sub-range discussed earlier.

5.1.1 Discrete filtering in multi-dimensions

In the case where filtering is required in more than one dimension over any topology, a box filtered function evaluated at node A is given as

$$\hat{f}(\boldsymbol{x}_A) = \frac{1}{\text{meas}(\Omega_A)} \int_{\Omega_A} f(\boldsymbol{y}) d\boldsymbol{y}. \tag{25}$$

where Ω_A is the union of elements which share node A. Here, the box filter kernel has been generalized such that at node A it becomes

$$G(\boldsymbol{x}_A, \boldsymbol{y}) = \begin{cases} \dfrac{1}{\text{meas}(\Omega_A)} & \text{if } \boldsymbol{y} \text{ is in } \Omega_A \\ 0 \text{ otherwise.} \end{cases} \tag{26}$$

In the case where filtering is performed over an evenly spaced quadrilateral or hexahedral mesh, quadrature approximations admit the sequential application of the one-dimensional discrete filters in each of the three principal directions. For example, in three dimensions we have

$$\hat{f}(x_0, y_0, z_0) = \sum_{i=-J}^{J} \sum_{j=-J}^{J} \sum_{k=-J}^{J} W_i W_j W_k f(x_i, y_j, z_k), \tag{27}$$

where the $\{y_j\}$ and the $\{z_j\}$ are spaced in the same manner as the $\{x_j\}$ defined earlier. Expanding the previous sum, the filtered function at the node (x_0, y_0, z_0) is seen to be given by a weighted combination of the function evaluated at neighboring quadrature points. The weights corresponding to each point add up to unity. The width of the three dimensional filter in (27) is defined as the width of its one dimensional counterpart.

In addition, it is possible to sequentially apply filters of different widths, for which the width of the resulting filter is taken often as

$$\hat{\Delta} = \left(\hat{\Delta}_1 \hat{\Delta}_2 \hat{\Delta}_3\right)^{1/3}, \tag{28}$$

where $\hat{\Delta}_i$ is the width of the filter applied in the i-th direction. In the case of elements with high aspect ratios, the width is taken as

$$\hat{\Delta} = \max\left(\hat{\Delta}_1, \hat{\Delta}_2, \hat{\Delta}_3\right). \tag{29}$$

For a detailed discussion on when it is appropriate to use either of the two previous expressions the reader is suggested to consult Deardoff [2] and Scotti *et al* [13], [14].

As discussed before, the test filter must be homogeneous in order to derive the dynamic model. Specifically, the test filter must be able to commute with differentiation. Errors induced by the non-commutivity between differentiation and discrete filtering operations such as (21) are of $O(\bar{\Delta}^2) = O(h^2)$, which is the same order as the spatial and temporal discretizations in the flow solver. A detailed discussion on the commutation errors of discrete filters is provided by Vasilyev [16].

In the case where two or three dimensional filtering is performed using unstructured (triangular, tetrahedral, non-uniform quadrilateral, or non-uniform

hexahedral) meshes, the generalized box kernel may not be symmetric; consequently, its width may not be obtainable from the formula in (3). Furthermore, in this case the box kernel may not be homogeneous, thus discrete approximations may induce large commutation errors. Later in this report we will show that discrete approximations of box filter on uniform tetrahedral meshes can work well in large-eddy simulations. In the near future we hope to show that these non-homogeneous discrete filtering operations introduce negligible commutation errors.

Furthermore, in the case of unstructured meshes, the quadrature rules used to evaluate the filtering operation in (25) does not yield filtered functions representable in the form of (27). However, still they result in a weighted combination of the function evaluated at the points surrounding that node at which the filtered function is evaluated. By construction, the weights corresponding to these points are non-negative and satisfy the normalization condition.

5.2 Finite dimensional filters as test filters

We hope to perform large eddy-simulations using higher order hierarchic basis functions in addition to the continuous piecewise linear basis functions currently used. The purpose for using higher order basis functions is to enable the efficient, accurate representation of turbulent flows on coarse meshes. If we use the box filter as the test filter in the same manner it was used in the previous sub-section, the resulting filter width will be greater than the inertial sub-range scales due to the coarseness of the meshes, thereby making the Smagorinsky model invalid. Thus, we need to define a special class of filters such that their widths fall on the inertial sub-range even on coarse meshes. For this, we make use of ideas discussed by Leonard [6] and Pope [11], who envision a filtered function as a finite dimensional projection of an infinite dimensional function.

Once again, consider a random function $f(x)$ characterized by high frequencies. The motivation for using finite dimensional projections of $f(x)$ as filters is that they can represent $f(x)$ up to certain scales. More precisely, the higher the order of the basis functions spanning the space being projected onto, the better the projected function can represent the smaller scales of $f(x)$. Such projections can be expressed as

$$\hat{f} = \sum_{n=1}^{N} a_n \phi_n(x), \tag{30}$$

where the members of the set $\{\phi_n\}_{n=1}^{N}$ are continuous piecewise polynomial basis functions and the set of coefficients $\{a_n(x)\}_{n=1}^{N}$ are to be determined.

5.2.1 Piecewise polynomial interpolations

One family of filters can be obtained by selecting the set of coefficients $\{a_n\}_{n=1}^{N}$ such that the filtered function interpolates the original function through N predetermined points. As an example of this type of filters, we take the filtered function $\hat{f}(x)$ to be the piecewise linear polynomial interpolating the original

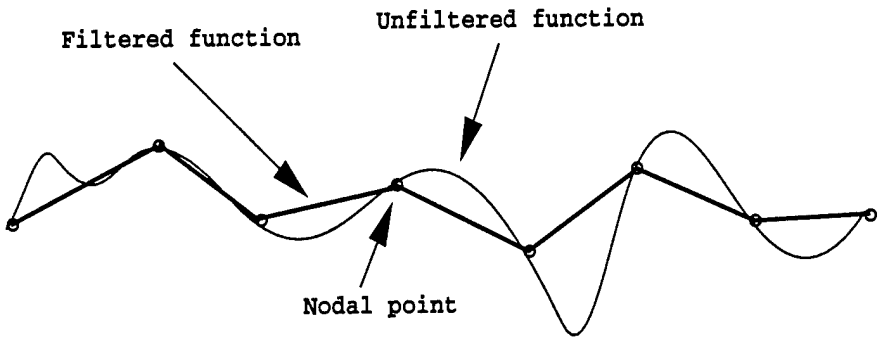

Figure 2: The effect of filtering using the kernel in (32) is shown.

function $f(x)$ through the mesh nodes:

$$\hat{f} = \sum_{n=1}^{N} f_n \phi_n(x), \tag{31}$$

where $f_n = f(x_n)$, N is the number of nodes in the mesh, and the set $\{\phi_n(x)\}_{n=1}^{N}$ consists of the Lagrangian continuous piecewise linear basis functions. The kernel associated to this filtering operation can be written as

$$\hat{G}(x,y) = \sum_{n=1}^{N} \delta(y - x_n)\phi_n(x). \tag{32}$$

Notice that this kernel is similar to those in (21), except that instead of constant weights it has variable weights. The homogeneity and symmetry of the kernel in (32) is still in question. However, this kernel works well in the large-eddy simulation of decaying isotropic turbulence. Similar to the generalized box filter on hexahedral (or quadrilateral) elements, we hope to show that the filtering operation brought about by (30) introduces negligible commutation errors.

A disadvantage in using kernels such as the one in (32) to compute the dynamic model coefficient in (20) is that gradients of the solution at mesh nodes are not continuous when the solution is piecewise linear or any other piecewise polynomial. However, we can overcome this obstacle by assuming that the required gradients at mesh nodes are averages over surrounding elements.

5.2.2 Least-squares (L_2) projections

A second family of filters can be obtained by determining the set of coefficients $\{a_n\}_{n=1}^{N}$ in (30) such that they minimize the square of the L_2-norm of the difference between the filtered and original functions over the domain of interest:

$$R = \frac{1}{L}\int_0^L (\hat{f}(x) - f(x))^2 \, dx, \tag{33}$$

where L is the distance of our domain. By substituting (30) into (33) and differentiating with respect to the $\{a_m\}$, it is seen that the coefficients satisfy

the matrix equation

$$\sum_{n=1}^{N} B_{mn} a_n = v_m, \tag{34}$$

with

$$B_{mn} = \frac{1}{L} \int_0^L \phi_m(x) \phi_n(x)\, dx, \tag{35}$$

and

$$v_m = \frac{1}{L} \int_0^L \phi_m(x) f(x)\, dx. \tag{36}$$

The family of filters in question admits the following family of kernels:

$$\hat{G}(x,y) = \sum_{n=1}^{N} \sum_{m=1}^{N} B_{mn}^{-1} \phi_n(x) \phi_m(y), \tag{37}$$

where B_{mn}^{-1} denotes the m-n entry of the inverse of the Gram (mass) matrix $\boldsymbol{B}$. It is important to note that the minimization of the integral in (33) could be performed over each mesh element, instead of the flow domain. In this case, the resulting filtered field would be discontinuous across elements.

Although the widths of the finite dimensional filters proposed are unclear, it should reflect the polynomial order of the basis functions employed. Clearly, higher order basis functions would yield smaller filter widths. Thus, unlike discrete filter widths, which are solely proportional to the mesh size, finite dimensional filter widths should depend on the chosen basis functions as well.

6 LES of Decaying Isotropic Turbulence

6.1 Decaying Isotropic Turbulence

Before moving on to a discussion of numerical results, let us take some time to review the essential aspects of our test problem. Under certain conditions, large-scale motions can become turbulent. In other words, the large-scale motions become unstable and break into smaller scale motions which take energy from the larger ones. Energy is passed down to such small scales at which it is dissipated by the action of molecular viscosity. At high enough Reynolds numbers, the small-scale motions cease to depend on the nature of the large-scale flow, leading to the universality of small-scale motions discussed in Section 3. Furthermore, these scales lose all directional orientation, in other words, they become isotropic. The energy contained in the sub-inertial scales (discussed in section 3) is characterized by what is usually referred to as the $five - thirds\ law$. In other words, the energy at these scales behaves as $k_r^{-5/3}$, where k_r represents the inverse of the size of the scales.

In the up-coming sub-sections we try to simulate a flow which is nearly isotropic at all scales. Our results are compared to the experimental data of Comte-Bellot and Corrsin [1], who tried to represent an infinite space of isotropic motions decaying in time because of a lack of kinetic energy production (in the absence of shear flows) to balance the viscous dissipation. They

accomplished this by obtaining a turbulence field behind a regular grid spanning a steady, uniform duct flow. By moving at the speed of the mean flow behind the grid, they correctly surmised that an observer would see something like true isotropic turbulence evolving in time.

6.2 Numerical observations

As can be seen in the dynamic Smagorinsky model, the filtered velocity field $\bar{u}$ depends on the ratio $\hat{\bar{\Delta}}/\bar{\Delta}$. The primary filter kernel, $\bar{G}$, appears implicitly in the equations, while the kernel $\hat{G}$ appears explicitly when computing the dynamic model. Essentially, the primary filter kernel as well as the kernel $\hat{\bar{G}}$ are arbitrary, yet their widths appear in the Smagorinsky model. Customarily, $\bar{\Delta}$ is given by the mesh spacing in a hexahedral mesh simulation:

$$\bar{\Delta} = (h_1 h_2 h_3)^{1/3} \tag{38}$$

or, in the case of elements with high aspect ratios,

$$\bar{\Delta} = \max(h_1, h_2, h_3), \tag{39}$$

where h_i is the mesh spacing in the i-th direction. The idea behind these choices is that they characterize the scales at the resolution threshold of the mesh. In reality, when the filtered equations are discretized, $\bar{\Delta}$ as well as $\hat{\bar{\Delta}}$ become dependent upon the numerical method of choice coupled with the effectiveness (or ineffectiveness) of the dynamic model, the mesh spacing, and the polynomial order of the basis functions used in the stabilized Galerkin approximation, which together act as the primary filter. In other words, $\bar{\Delta}$ in (38) is perturbed in the form

$$\bar{\Delta} = \epsilon (h_1 h_2 h_3)^{1/3}, \tag{40}$$

where $\epsilon \approx 1$ is a constant depending on the numerical method, the model, the mesh, and the polynomial order of the basis functions underlying the method. Thus, we are left with a difficult question: How can we evaluate $\bar{\Delta}$ and $\hat{\bar{\Delta}}$ correctly? More precisely, how can we compute the ratio $\hat{\bar{\Delta}}/\bar{\Delta}$ correctly? In section 4, we showed how to calculate $\hat{\Delta}$ for discrete test filters on a uniform hexahedral mesh. Here we make use of this information in assuming that for a hexahedral mesh

$$\beta = \frac{\hat{\bar{\Delta}}}{\bar{\Delta}} = \kappa \left(\frac{\hat{\Delta}_1 \hat{\Delta}_2 \hat{\Delta}_3}{h_1 h_2 h_3} \right)^{1/3}, \tag{41}$$

where κ is a positive constant and β is the filter width ratio (FWR). The parameter κ serves to characterize the unknown filter width $\bar{\Delta}$.

In the decay of isotropic turbulence, the scales of motion are isotropic and vary over the same range everywhere in the domain. Periodicity can be assumed in the three principal directions as long as the two-point spatial autocorrelations of velocities over distances equivalent to the domain length vanish. Given these characteristics of the flow in question, we can ascertain that for

an evenly spaced hexahedral mesh with no *p-refinement* the numerical procedure resolves turbulent motions larger than a constant scale $\bar{\Delta}$. (Otherwise, if we were to perform *p-refinement* or *h-refinement* in some regions of this flow, the numerical procedure would resolve up to scales smaller than in other regions, yielding a non-constant $\bar{\Delta}$.) Moreover, $\hat{\Delta}$ is constant as well because we are using an evenly spaced mesh. Thus, $\hat{\bar{\Delta}}$, which depends on $\bar{\Delta}$ and $\hat{\Delta}$, is taken as constant. Now it should be clear that for decaying isotropic turbulence simulated on an evenly spaced hexahedral mesh with no *p-refinement*, the expression in (41) is consistent in the sense that both of its sides are constants throughout the flow domain.

To verify the validity of (41), we performed the simulation with two different test filters on a fixed evenly spaced hexahedral mesh using continuous piecewise linear basis functions. For each case, the filter width ratio was expressed as:

$$\frac{\hat{\bar{\Delta}}_1}{\bar{\Delta}} = \kappa \frac{\hat{\Delta}_1}{h} \quad \text{and} \quad \frac{\hat{\bar{\Delta}}_2}{\bar{\Delta}} = \kappa \frac{\hat{\Delta}_2}{h}. \tag{42}$$

Here the subscript on the filter width denotes the first or second simulation. Note that no distinction is made between the filters applied in different directions because we are dealing with an evenly spaced mesh (i.e.,. $h = h_1 = h_2 = h_3$). Furthermore, no distinction is made for $\bar{\Delta}$ between the first and second simulations arguing that because the uniform mesh is fixed, $\bar{\Delta}$ remains constant as was discussed earlier. However, one might also argue that because the test filter changes the numerical method changes as well, consequently, $\bar{\Delta}$ changes. Later we will see that this is not the case as long as the test filter widths, $\hat{\Delta}_1$ and $\hat{\Delta}_2$, are consistently calculated using (24). Thus, because the constant κ characterizes $\bar{\Delta}$, it remains constant as well from simulation to simulation. In summary, we will see that both $\bar{\Delta}$ and κ are independent of the test filter used as long as the test filter width is accurately computed.

When the simulation is performed with a uniform tetrahedral mesh, the assumption made in (41) is not feasible because $\hat{\Delta}$ is not well-defined. However, we can measure the constant

$$\beta = \frac{\hat{\bar{\Delta}}}{\bar{\Delta}} \tag{43}$$

for which the simulation performs well with respect to experimental data. Note that the best value of β is particular to the test filter. Furthermore, in setting (43) as a constant we have assumed that for an uniform tetrahedral mesh with no *p-refinement*, Δ is constant throughout the flow domain, as was discussed earlier.

In the case of more complex flows, where the scales of motion might vary from region to region, *h-refinement* and *p-refinement* are often employed to improve local resolution. If these refinements are made, no longer are $\bar{\Delta}$, $\hat{\Delta}$, and $\hat{\bar{\Delta}}$ constants over the domain; instead, they reflect the local mesh spacing and local polynomial order. However, if we were to refine such that both sides of (41) or the left hand hand side of (43) remain constants, the consistency of these expressions should hold, at least approximately. Their validity should be verified. Furthermore, $\bar{\Delta}$ and $\hat{\bar{\Delta}}$ should be varied slowly enough such that they can be approximated as locally constant in the derivation of the dynamic model.

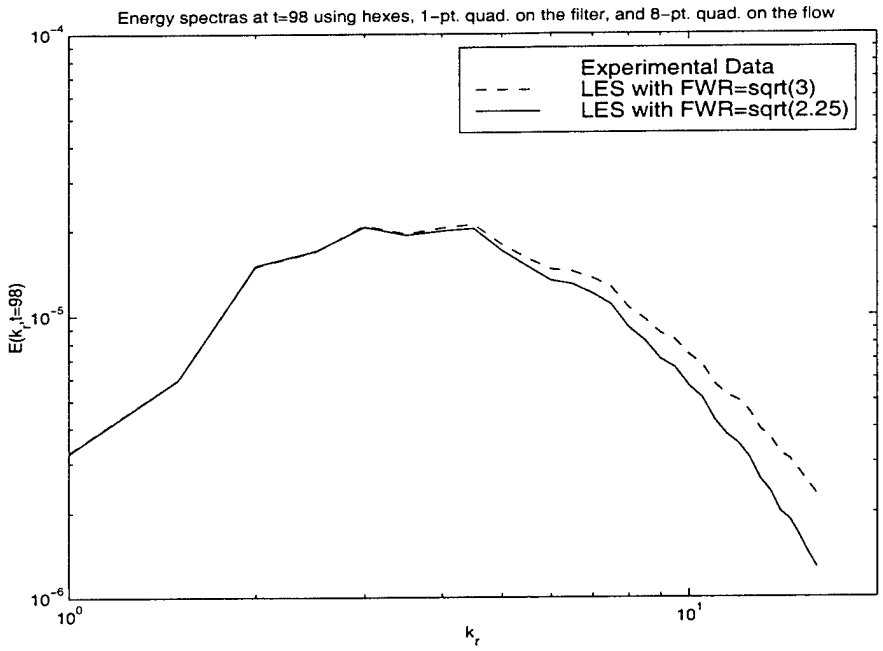

Figure 3: LES of decaying isotropic turbulence performed with hexahedral elements. FWR (filter width ratio) = β.

6.3 Numerical results

Two sets of simulations of decaying isotropic turbulence were performed using an evenly spaced linear hexahedral mesh discretizing a cubic domain with sides of length 2π and subjected to periodic boundary conditions in the three principal directions. The two sets are distinguished solely by a change in the discrete test filter. In the first set, the test filter is taken as the box filter approximated by one-point quadrature. In the second set, the test filter is taken as the box filter approximated by eight-point quadrature.

The length of the mesh spacings was taken as $h = 2\pi/32$, where 32 is the number of space intervals in each direction. Furthermore, as mentioned earlier, the results are compared to experimental data. However, since the results are in terms of primary filtered variables (i.e., $\bar{u}$), the experimental data used for comparison should also be filtered. The filtering of the experimental data should be of width $\bar{\Delta}$, however, since this value is not available to us, we picked it to be $O(h)$, specifically, $\bar{\Delta} = h$.

6.3.1 Box filter on hexes approximated by one-point quadrature

The first set of simulations was performed with the test, box filter approximated by a one-point quadrature rule yielding a discrete filter of width $\hat{\Delta} = \sqrt{3}\ h$. First, κ in (41) was set to unity, yielding a filter width ratio $\beta = \sqrt{3}$. Then κ was set to any number, here taken as $\sqrt{9/12}$, yielding a filter width ratio $\beta = \sqrt{9/4} = \sqrt{2.25}$. The results of this set of simulations are plotted in Figure

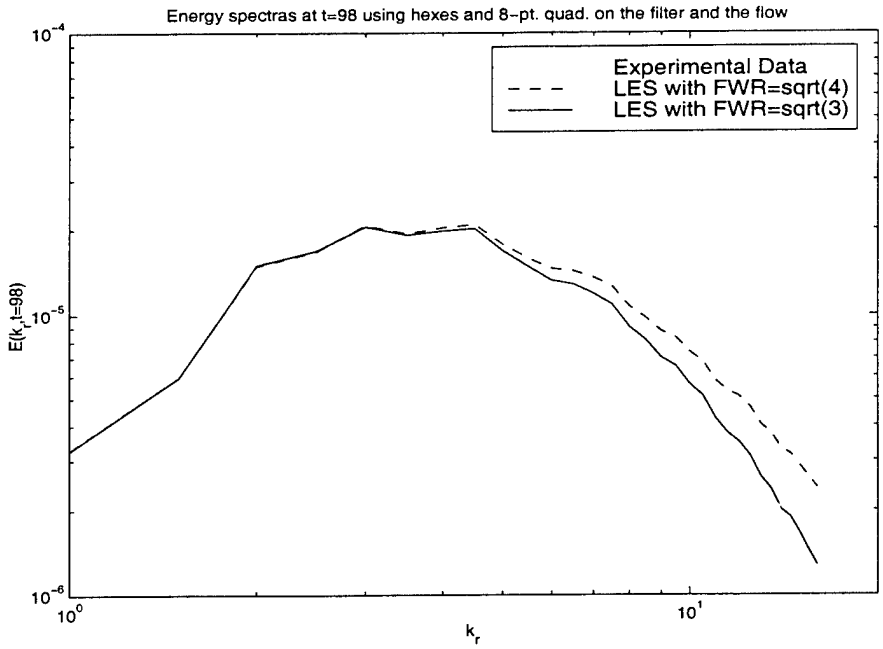

Figure 4: LES of decaying isotropic turbulence performed with hexahedral elements.

3.

6.3.2 Box filter on hexes approximated by eight-point quadrature

The second set of simulations was performed using the test (or box) filter approximated by an eight-point quadrature rule, yielding a discrete filter of width $\hat{\Delta} = 2h$. First, κ was set to unity, yielding a filter width ratio $\beta = \sqrt{4}$. Then, once again, κ was reset to $\sqrt{9/12}$, yielding a filter width ratio $\beta = \sqrt{3}$. The results of this set of simulations are plotted in Figure 4.

Looking at Figures 3 and 4, we see that results do not vary from simulation to simulation as long as the test filter widths are consistently calculated using (24). We ascertain that the test filter does not have an impact on the results as long as its width is accurately represented. Furthermore, we can say that $\bar{\Delta}$ remained constant from simulation to simulation as was assumed before and that the parameter κ strictly characterizes the unknown primary filter width $\bar{\Delta}$ independent of the test filter used. In addition, the ratio β scales as $O(\bar{\Delta}/\Delta)$ for this problem and the parameter κ can be adjusted so as to obtain preferable results.

6.3.3 LES on tetrahedral elements

The simulation of decaying isotropic turbulence was also performed with uniform tetrahedral elements discretizing the domain discussed in the previous paragraph. As mentioned earlier, a proper value of β in this case is not within our means, thus we chose to keep this value fixed at $\sqrt{3}$ for all simulations. How-

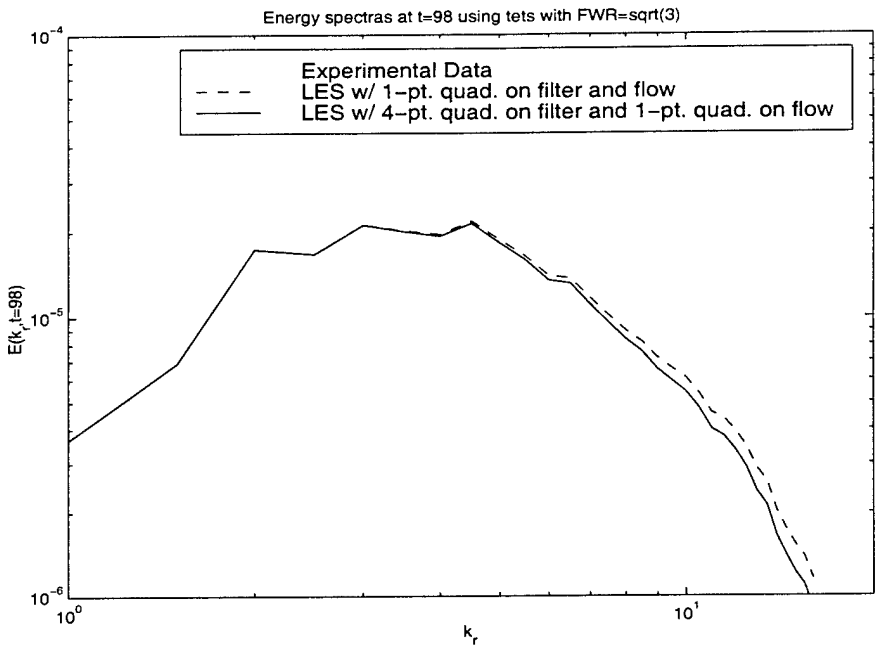

Figure 5: LES of decaying isotropic turbulence performed with tetrahedral elements and $\beta = \sqrt{3}$.

ever, we varied the quadrature rule used to approximate the box filter and the quadrature rule used to integrate the discretized flow equations (which alters the numerical method). Although not shown in the figures, a slight variation of β affects the energy spectra shown in Figures 5 and 6, thus a value of β can be obtained such that the simulation nearly matches experimental results. In the future we hope to arrive at a concrete way of calculating the best choice for β. Of greater importance is that despite the possible non-homogeneity and non-symmetry of the generalized box filter on tetrahedral elements, discrete approximations of said filter are shown to work just as well as discrete approximations of the generalized box filter on hexahedral elements, for which homogeneity and symmetry are well established.

6.3.4 An approximate least-squares projection

In Figure 7 we show results of the simulation performed with the least-squares projection filter whose kernel appears in (37). This filter operator was approximated by lumping of the Gram (or mass matrix) and using one-point quadrature. Here we have chosen $\beta = \sqrt{3}$, for which the simulation performed well with hexahedral elements. Choosing $\beta = \sqrt{4}$ produces even better results. However, in the future we would like to establish a rigorous way of how to choose the appropriate value of β. Although not shown, the simulation also performed well with tetrahedral elements.

Note that in this simulation filtered functions where evaluated in the interior of the elements, unlike the simulations performed with the discrete box filter in which the filtered functions were evaluated at the mesh nodes. The reason for

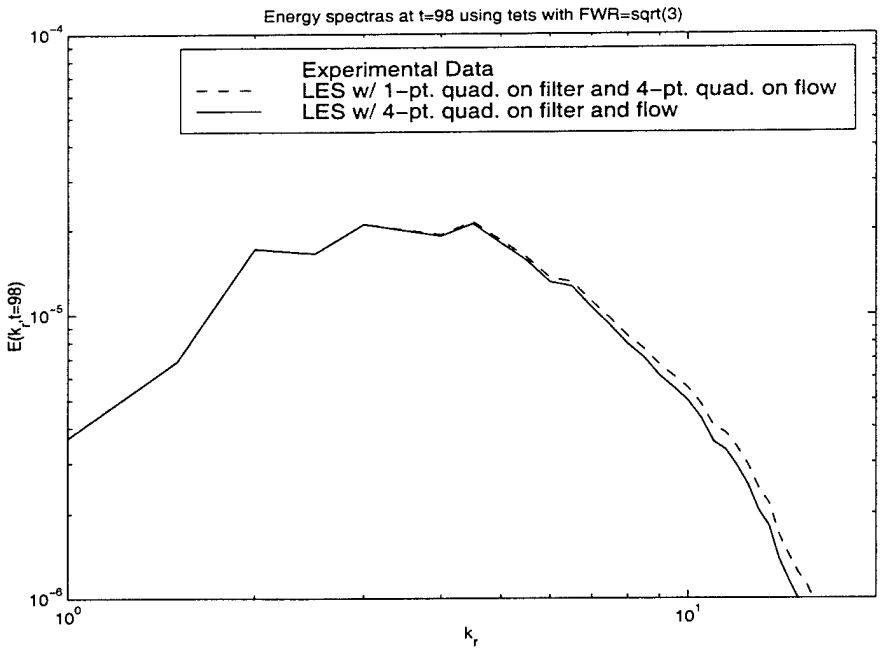

Figure 6: LES of decaying isotropic turbulence performed with tetrahedral elements and $\beta = \sqrt{3}$.

this variation is that the least-squares filter operator under the lumping and one-point quadrature approximations reduces to the box kernel approximated by one-point quadrature when both are used at the mesh nodes.

6.4 Initial conditions and implementational details

Experimental data is available from [1], however, it is not enough to create a fully turbulent initial condition for the simulations. From the data we were able to obtain the correct amplitudes of the flow velocities in wavenumber space at two dimensionless time stations, namely $t = 42$ and $t = 98$. As an approximate initial condition we used the experimental velocity amplitudes at $t = 42$, at discrete points in wavenumber space corresponding to discrete points in real space; the corresponding phases where assigned random numbers. These velocities where then used to compute a pressure field satisfying the Poisson equation for pressure in wavenumber space. The inverse Fourier transform was used to obtain real initial conditions. However, these initial conditions were not appropriate due to the random phases assigned to the velocities. The simulation was run for a couple of hundreds time steps. The resulting velocities where then transformed back to wavenumber space and their phases extracted and re-assigned as the phases of the experimental velocity amplitudes at $t = 42$. The simulation was re-run until iterations of the procedure previously outlined produced the same results, signaling that an appropriate (fully turbulent) initial condition had been obtained.

As was mentioned earlier, the finite element solver employed uses the Stream-

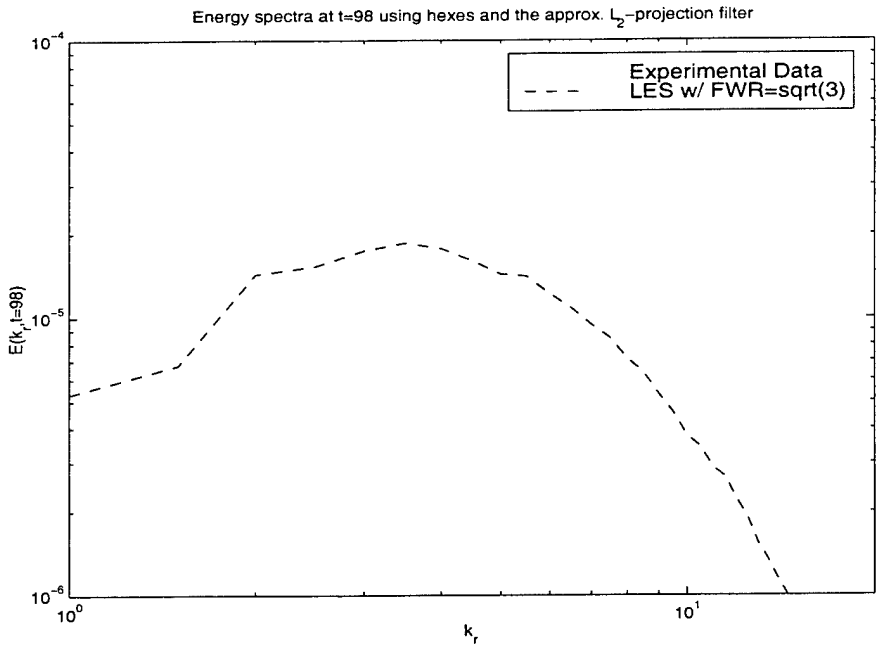

Figure 7: LES of decaying isotropic turbulence using an approximation of the least-squares (L_2) projection as the test filter and $\beta = \sqrt{3}$.

line Upwind Petrov-Galerkin (SUPG) method. The large eddy-simulations in this report were performed using incompressible (see [18]) and compressible (see [4]) versions of the solver. The compressible simulations were performed with a Mach number much less than unity in order for the flow to approach incompressibility. Furthermore, the compressible solver was used in its incompressible limit. Results from both of the cases using the compressible solver matched the results of the incompressible solver.

For clarity issues, in this report the dynamic Smagorinsky model was derived in its incompressible form. For compressible flows the Smagorinsky model varies slightly. The interested reader is encouraged to consult [10] for a derivation of the compressible version of the model. This compressible version reduces to the incompressible form by setting density equal to a constant.

6.5 Conclusions

Large-eddy simulation using a dynamic residual stress model proved to be successful when extended to unstructured meshes using a generalized box filter as the test filter. Simulation results were shown to be independent of the test filter provided the test filter width is consistently represented. We hope to further validate the role of the parameter κ, characterizing the unknown primary filter width, by performing the simulation on finer meshes. Furthermore, possible alternative filters to the generalized box filter were introduced. These finite dimensional filters, based on continuous piecewise polynomial approximations and least-squares projections, would be preferred for higher order large-eddy

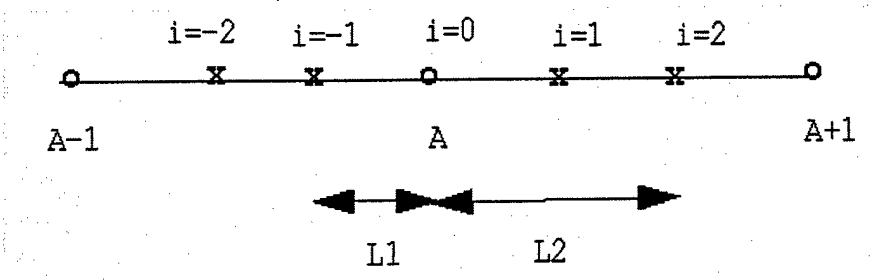

Figure 8: Schematic for a discrete approximation to a box filtered function.

simulations on coarse meshes. In the near future we hope to estimate the homogeneity of the generalized box filter and the finite dimensional filters.

7 Appendix I

Here we will show some calculations done when computing a box filtered function using the well known 2-point Gaussian quadrature rule. Consider the schematic in figure 8 as we set out to obtain the filtered function $\hat{f}$ evaluated at node A or 0. Here $x_A - x_{A-1} = x_{A+1} - x_A = h$, $L_1 = h \cdot \alpha_1 = h \cdot 0.211$ and $L_2 = h \cdot \alpha_2 = h \cdot 0.788$ Thus, we have

$$\hat{f}(x_A) = \hat{f}(x_0) = \sum_{i=-2}^{2} W_i f(x_i), \tag{44}$$

where $W_i = 1/4$ for all i. This discrete filter yields a filter kernel of the form

$$\hat{G}(x-y) = h \sum_{i=-2}^{2} W_i \delta(x - y + \alpha_i). \tag{45}$$

Inserting the values for W_i and α_i with $J = 2$ into the expression in (24) we find that the width of the filter kernel in (45) is $\hat{\Delta} = 2h$.

References

[1] G. Comte-Bellot and S. Corrsin. Simple Eulerian time-correlation of full and narrow-band velocity signals in grid-generated 'isotropic' turbulence. *Journal of Fluid Mechanics*, 48:273–337, 1971.

[2] J. W. Deardorff. A numerical study of three-dimensional turbulent channel flow at large Reynolds numbers. *Journal of Fluid Mechanics*, 41:453, 1970.

[3] M. Germano. Turbulence: the filtering approach. *Journal of Fluid Mechanics*, 238:325–336, 1992.

[4] K. E. Jansen. A stabilized finite element method for computing turbulence. *Comp. Meth. Appl. Mech. Engng.*, 174:299–317, 1999.

[5] K. E. Jansen, C. H. Whiting, and G. M. Hulbert. A generalized-α method for integrating the filtered Navier-Stokes equations with a stabilized finite element method. *Comp. Meth. Appl. Mech. Engng.*, 1999. Contributed to a special volume devoted to the Japan-US Symposium on F.E.M. in Large-Scale C.F.D., SCOREC Report 10-1999.

[6] A. Leonard. On the energy cascade in large-eddy simulations of turbulent fluid flows. Technical report, Stanford University, 1973.

[7] D. K. Lilly. On the application of the eddy viscosity concept in the inertial subrange of turbulenc. Boulder, Colorado, 1966. NCAR Manuscript 123.

[8] D. K. Lilly. A proposed modification of the Germano subgrid–scale closure. *Physics of Fluids*, 3:2746–2757, 1992.

[9] T. S. Lund. On the use of discrete filters for large-eddy simulation. In *Annual Research Briefs*, pages 83–95, NASA Ames / Stanford University, 1997. Center for Turbulence Research.

[10] P. Moin, K. Squires, W. H. Cabot, and S. Lee. A dynamic subgrid–scale model for compressible turbulence and scalar transport. *Physics of Fluids*, 3:2746–2757, 1991.

[11] S. B. Pope. Large-eddy simulation using projection onto local basis functions. In J. L. Lumley, editor, *Fluid Mechanics and the Environment: Dynamical Approaches*. Springer, 2000. To appear.

[12] S. B. Pope. *Turbulent Flows*. To appear, 2000.

[13] A. Scotti and C. Meneveau. Generalized smagorinsky model for anisotropic grids. *Physics of Fluids A*, 5:2306–2308, 1993.

[14] A. Scotti, C. Meneveau, and M. Fatica. Dynamic smagorinsky model on anisotropic grids. *Physics of Fluids*, 9:1856–1858, 1997.

[15] J. Smagorinsky. General circulation experiments with the primitive equations, I. The basic experiment. *Monthly Weather Review*, 91:99–152, 1963.

[16] O. V. Vasilyev and T. S. Lund. A general theory of discrete filtering for les in complex geometry. In *Annual Research Briefs*, pages 67–82, NASA Ames / Stanford University, 1997. Center for Turbulence Research.

[17] A. W. Vreman, B. J. Geurts, and J. G. M. Kuerten. On the formulation of the dynamic mixed subgrid-scale model. *Physics of Fluids*, 6:4057–4059, 1994.

[18] C. H. Whiting and K. E. Jansen. A stabilized finite element method for the incompressible Navier-Stokes equations using a hierarchical basis. *International Journal of Numerical Methods in Fluids*, accepted, 1999. SCOREC Report 9-1999, Scientific Computation Research Center, Rensselaer Polytechnic Institute, Troy, NY.

[19] Y. Zang, R. L. Street, and J. R. Koseff. A dynamic mixed subgrid-scale model and its application to turbulent recirculating flows. *Physics of Fluids A*, 5:3186, 1993.